Simultaneous Measurement of the Dissolution Kinetics of Responsive DNA Hydrogels at Multiple Length Scales

Journal:	*ACS Nano*
Manuscript ID	nn-2016-06414q.R2
Manuscript Type:	Article
Date Submitted by the Author:	n/a
Complete List of Authors:	Simon, Anna; University of California Santa Barbara, Biomolecular Science and Engineering Program Walls-Smith, Luke; University of California Santa Barbara, Department of Chemistry and Biochemistry Freddi, Matthew; University of Kent, Medway School of Pharmacy Fong, Faye; University of California Santa Barbara, Department of Materials Gubala, Vladimir; University of Kent, Medway School of Pharmacy Plaxco, Kevin; University of California, Santa Barbara, Department of Chemistry and Biochemistry

Simultaneous Measurement of the Dissolution Kinetics of Responsive DNA Hydrogels at Multiple Length Scales

Anna J. Simon[1‡], Luke T. Walls-Smith[2], Matthew J. Freddi[5], Faye Yi Fong[3], Vladimir Gubala[5], and Kevin W. Plaxco[1,2,4]*

[1]Biomolecular Science and Engineering Program, University of California Santa Barbara, Santa Barbara, CA 93106-9010 USA

[2]Department of Chemistry and Biochemistry, University of California Santa Barbara, Santa Barbara, CA 93106-9010 USA

[3]Department of Materials, University of California Santa Barbara Santa Barbara, CA 93106-9010 USA

[4]Center for Bioengineering, University of California Santa Barbara Santa Barbara, CA 93106-9010 USA

[4]Medway School of Pharmacy, University of Kent, Central Avenue, Chatham Maritime, Chatham, ME4 4TB, Kent, UK

Corresponding Author: *Kevin W. Plaxco, kwp@chem.ucsb.edu

‡**Present Address:** ‡AJS: Center for Systems and Synthetic Biology, University of Texas at Austin, Austin TX 78705

Keywords: rheology, smart materials, aptamers, macromolecular assemblies, gels, soft matter

Abstract: Recent years have seen increasing study of stimulus-responsive hydrogels constructed from aptamer-connected DNA building blocks. Presumably due to a lack of simple, quantitative tools with which to measure gel responsiveness, however, the literature describing these materials is largely qualitative. In response we demonstrate here simple, time-resolved, multi-scale methods for measuring the response kinetics of these materials. Specifically, by employing trace amounts of fluorophore-quencher labeled crosslinkers and the rheology of entrapped fluorescent particles we simultaneously measure dissolution at molecular, hundred-nanometer, and hundred-micron length-scales. For our test-bed system, an adenine-responsive hydrogel, we find biphasic response kinetics dependent on both effector concentration and depth within the gel and a dissolution pattern uniform at scales longer than a few times the monomer-monomer distance. Likewise, we find that, in agreement with theoretical predictions, dissolution kinetics over the hundred nanometer length scale exhibit a power-law-like dependence on the fraction of disrupted crosslinks before a distinct crossover from solid-like to liquid-like behavior.

The stimulus-responsive materials found in biology are typically composed of precisely organized biomolecular networks that assemble, dissolve, and rearrange in response to specific molecular cues.[1-5] To create similarly responsive artificial materials many researchers have turned to DNA as its simple base-pairing rules support the ready design of precisely organized three-dimensional hydrogels.[6-13] Moreover, by incorporating aptamers, artificial sequences selected for their ability to bind specific molecular effectors, these hydrogels can be made responsive to many specific cues ("effectors"), including, to date, pH,[7,8] mercury,[9] adenosine,[9,10] cocaine,[10] lead,[10] thrombin,[11] silver,[12] and sequence-specific endonucleases.[13]

The simplicity with which responsive DNA hydrogels are designed and the potentially broad range of effectors to which they may respond have motivated significant study (*e.g.*, refs[7-13]). The majority of this literature, however, has proven rather qualitative, with little work having described, for example, the kinetics with which these hydrogels respond as functions of parameters such as the effector concentration, position within the hydrogel, or length scale over which dissolution is monitored. This is unfortunate because the development of strategies for the rational optimization of responsive hydrogels will likely require quantitative understanding of their physical properties. For example, although theoretical[14-16] and simulation-based predictions[17-24] and indirect experimental studies[25-30] regarding the interplay between molecular scale crosslinker dissociation and larger-scale mechanics exist, direct experimental tests of these relationships are lacking.[31,32] In response, we demonstrate here methods for the measurement of the response kinetics of DNA hydrogels at length scales ranging from molecular through nanometer to hundreds of microns. As proof of principle we have employed these methods to measure the dissolution kinetics of a model aptamer-based hydrogel as functions of effector concentration and the depth (within the hydrogel) and the length scale over which dissolution is

observed. The resultant data provides a means of testing several previously predicted physical properties of such responsive hydrogels, demonstrating the utility of our approaches for improving our understanding of and ability to optimize this important class of materials.

Results and Discussion:

As our model system we have employed a Y-DNA hydrogel architecture responsive to the effector adenosine. First described in 2009 by Cheng *et al*.,[7] these responsive Y-DNA hydrogels consist of networks of Y-shaped "monomers" (each containing three strands forming a double-stranded core with three pendant arms) crosslinked *via* hybridization to a complementary sequence (Figures 1, S1). For our studies we used the 27-base adenosine-binding aptamer of Huizenga and Szostak[33] as this crosslink, rendering the resulting hydrogel responsive to this molecular stimulus. The DNA secondary structure prediction software Mfold[34,35] predicts that this aptamer forms a stable hairpin conformation with a favorable free energy of 7.3 kJ/mol even in the absence of adenosine (corresponding to >90% of the population in the hairpin configuration). Mixing the aptamer (at 490 μM) with the two Y-monomers (185 μM each) produces an observably thick, rigid hydrogel, consistent with previous[13] bulk rheological studies of analogous Y-DNA hydrogels (Figure 1, B, C). The introduction of adenosine, which stabilizes the aptamer's hairpin-like "native" conformation, dissociates the crosslinks and thus dissolves the hydrogel (Figure 1, A). As previously reported, this can be observed qualitatively by eye (see, *e.g.*, refs[6-13]). Our goal, however, is to instead develop quantitative methods of monitoring dissolution over multiple length scales.

Key to our studies is the ability to simultaneously monitor the gel's response to its effector over a wide range of length scales. Specifically, to measure the gel's molecular-scale dissolution

kinetics we employ a trace (~1%) amount of aptamer modified by the addition of a fluorophore-quencher pair attached to its termini (Figure 1, D, E). When the aptamer sequence is acting as a crosslink the fluorophore and quencher are separated by ~9 nm (14 base-pairs of double-stranded DNA and 13 bases of single-stranded DNA).[36] As this separation significantly exceeds the Förster radius of the fluorophore-quencher pair, emission is high **(**Figure 1, D). In the presence of adenosine, however, the aptamer's conformational equilibrium favors its dissociation and folding (into its adenosine-bound conformation), bringing the fluorophore into proximity with the quencher and reducing emission[33] (Figure 1, E). Thus, fluorescence provides a ready means of monitoring dissolution at the molecular scale. To monitor dissolution at longer length scales we use passive rheology, a method commonly employed for measuring the mechanics of soft materials.[37] Specifically, we measure the mobility of beads (of diameter 210 nm to 3.2 μm) embedded in the hydrogel as a function of time after the addition of an adenosine-containing solution to the top of a ~2 μl volume of gel in a simple, transparent flow channel through which the beads and aptamer fluorescence can be observed (Figure S2). Initially, the intact hydrogel restricts the movement of the beads so that they "jiggle" in place only slightly in response to thermal fluctuations. As the network dissolves, the mobility of the beads increases, eventually reaching that expected for unhindered Brownian diffusion through water. Finally, whole-gel imaging provides a means of simultaneously monitoring the cooperativity of the dissolution process over the hundreds of micrometer field of view of our microscope.

Time-lapse images capturing the fluorescence of labeled aptamers indicate that the hydrogel's molecular-scale dissolution kinetics are biphasic, with a slow initial decrease in fluorescence (the "lag phase") followed by a near-exponential decrease (the "exponential phase") (Figure 2). The lengths of both of these phases are strongly concentration-dependent. Specifically, at a depth of

450 μm within the sample, the lag phase t_{lag} (here defined as the time required to reduce background-subtracted fluorescence by 5%) increases 3-fold from 1.6±0.4 min to 4.2±0.1 min as the adenosine concentration drops 70-fold from 14 mM to 0.2 mM. The lifetime (time constant) of the exponential phase (obtained by fitting the trace obtained after the normalized fluorescence has decreased to 75% of its initial value) depends still more strongly on adenosine concentration, increasing 7-fold (from 5.5±0.4 min to 38.3±0.1 min) over this same range (Figure 2, C). Correspondingly, the time required for the entire process (the lag and exponential phases acting together) to reduce the fluorescence to 50% of its initial value ($t_{1/2}$) likewise depends strongly on concentration, increasing 7-fold (from 5.3±0.6 min to 37.2±6.1 min) over this same range of effector concentrations.

Not surprisingly, the kinetics of dissolution also depend on the depth within the gel at which dissolution is monitored (Figure 3). The dependence arises, however, solely due to changes in the lag phase; the lifetime of the exponential phase appears to be effectively independent of depth. In response to 6 mM adenosine, for example, the length of the lag phase increases 3-fold from (0.6±0.2 min to 1.8±0.1 min) as the depth within the sample increases from 300 μm to 600 μm, an effect that presumably arises due to the finite time required for the effector to diffuse into the material.[23] The lifetime of the exponential phases, in contrast, are effectively indistinguishable at all depths we have monitored (Figure 3, C).

The final fluorescence we observe plateaus at near background levels after less than 150 min at all effector concentrations, suggesting that, at equilibrium, even the lowest concentration (0.2 mM) of adenosine we have employed leads to near complete dissolution of the hydrogel. This observation was unexpected; binding must "outcompete" the hybridization of the aptamer to the monomers, which, based on zeroth order calculations of the DNA hybridization

thermodynamics, we believed would push the aptamer's dissociation constant far above this concentration, precluding complete dissociation. Specifically, using Mfold[34, 35] we estimate that the stability of the aptamer-Y-monomer base-pairing is -60 kJ/mol. Constraining the non-binding portion of the aptamer, however, is entropically unfavorably, and carries an energetic cost roughly equivalent to constraining the ends of a non-base pairing loop of a hairpin, which Mfold and excluded-volume polymer theory predict to be ~13 kJ/mol.[34, 35, 38] In total we would expect these to reduce the energy of adenosine binding by 47 kJ/mol relative to the binding of the free aptamer, which should increase the 6 μM K_{half} of the aptamer[33] by eight orders of magnitude. The near complete dissociation seen at 0.2 mM adenosine suggests, however, that the actual K_{half} is significantly less than 3 orders of magnitude above that of the free aptamer. This discrepancy likely arises largely due to the unfavorable entropic cost of arranging the Y-monomers and aptamer into the hydrogel network.[39] From the approximately five order of magnitude difference between the expected and experimentally estimated K_{half} of adenosine we estimate the additional "cost" associated with forming the hydrogel as 30 kJ/mol, which is roughly consistent with previous estimates of the entropic cost of forming such assemblies.[40]

While the dissolution of the hydrogel as measured over length scales of a few hundred nanometers to a few micrometers shares the same biphasic lag-and-exponential pattern as dissolution at molecular length scales, it is orders of magnitude slower and significantly more concentration-dependent. For example, when we employ the mobility of 1.0 μm beads as our reporter, the lag phase, which we define here as the time required for the mean square displacement to exceed 10% of that expected in buffer, increases more than 30-fold from 5.9±0.3 min to greater than 2 hr as the adenosine concentration drops from 14 mM to 0.2 mM (Figure 4). The lifetimes of the exponential phase similarly increase from τ = 9.4±1.6 min at 14 mM to

much greater than 2 hr at adenosine concentrations below 2 mM. The half-life of the overall dissolution process (defined for here as the time required for the mean squared displacement to reach half the value expected in buffer) correspondingly increases from $t_{1/2}$ = 11.6±2.0 min to greater than 120 min at or below 2 mM (Figure 4, C).

The nanometer-to-micrometer-scale dissolution kinetics of our hydrogels vary only modestly as a function of the size of the bead employed in the measurements (Figure 5). Specifically, the half-time of the overall dissolution changes by only a factor of three (from $t_{1/2}$ = 11.6±0.8 min to $t_{1/2}$ = 29.5±1.7 min) as the bead diameter increases nearly 15-fold from 210 nm to 3.2 μm (Figure 5, C). The relatively weak bead-diameter-dependencies we do observe arise due to changes in the lag time, which increases about 3-fold (from t_{lag} = 5.5±0.8 min to t_{lag} = 15.8±1.4 min) over this same 15-fold increase in bead diameter. The lifetime of the exponential phase, in contrast, increases less than 2-fold (from τ = 23.0±1.5 min to τ = 34.8±2.9 min) over this increase. The increase in lag time with increasing bead size suggests that, early in dissolution, the mesh size of the gel increases to enable increased movement of smaller beads, while nevertheless remaining sufficiently intact to trap the larger beads. Once the mesh size has decreased sufficiently to enable the movement of larger beads, however, the network has approached complete dissolution, resulting in a relatively small difference in the exponential phase for the larger beads.

In addition to providing a measure of the dissolution kinetics and thermodynamics of the hydrogel, our approach also allows us to visualize the progression of its dissolution over time and space, thus providing an experimental view into the underlying mechanism (Figure 6). The extent to which neighboring bonds affect each other in multivalent assemblies, for example, has long been an area of theoretical study[41,42] that we can test by looking for variations in dissolution

across our field of view. Doing so we find that the gel exhibits a steady, even decrease in fluorescence over the entire 169 μm by 169 μm field of view, suggesting that crosslinkers dissociate from this model hydrogel randomly over time. This observation stands in contrast to patterns we would expect to see if dissolution were highly cooperative with areas of initial dissolution propagating over time, which would presumably produce a patchy, punctate decreases in fluorescence, with dark spots forming and expanding at their edges, or a wave-front pattern in which dissolution progresses from one side to the other.

Our ability to measure both the hydrogel's molecular scale dissolution and the extent to which it inhibits the motion of nanometer-to-micrometer beads simultaneously also provides an opportunity to test prior theories relating a gel's crosslinking to its bulk mechanical properties, including gelation and percolation theory.[14-22] Key to this theory is the percolation threshold, p_c, a unit-less parameter defined as the minimum fraction of intact crosslinkers for which there exists a continuous connected path through the gel. The theory predicts that above p_c a power law relationship exists between the number of intact bonds and the mean square displacement of an object much larger than the gel spacing. Below this threshold, in contrast, the gel network structure is no longer sufficiently intact to trap such an object, and thus the mean squared displacement increases only moderately as the breakage of further bonds decreases the viscosity of the now liquid environment.

Simulations of mechanical properties of simple model gels[17-24] support this theory, as do some prior experimental studies that measured only the micron-scale dissolution of the gel without simultaneously quantifying the number of crosslinks (*i.e.*, without measuring p_c).[25-30] The simultaneous measurement of both thus produces more quantitative testing of this theory. From these measurements we find that, for adenosine concentrations ranging from 2 to 14 mM, a plot

of the normalized fluorescence (which captures the number of intact bonds) *versus* mean squared bead displacement is biphasic, with an early power law-like phase transitioning into a plateau as the extent of dissolution increases and the hydrogel becomes liquid-like (Figure 7). And while the distinct, phase-like nature of this transition is consistent with previous theoretical[14-24] and experimental[25-30]observations, the simultaneous measurement of both molecular- and micron-scale dissolution probes this transition directly. Specifically, we find that, consistent with the prediction of Flory-Stockmayer critical gel point p_c for networks composed of trivalent monomers, the rather distinct crossover between the two behaviors occurs when ~50% of the crosslinkers are broken (*i.e.*, when ~50% of the total fluorescence change has occurred). Our results are likewise quantitatively consistent with the theoretical prediction[19-20] that the power-law behavior seen before this transition exhibits an exponent of ~3.8 (Figure 7).

In contrast to the above observations, the behavior we observe at lower effector concentrations (below 2 mM) do not produce the same power-law-to-liquid transition. That is, even when >50% of crosslinkers are dissociated under these conditions, bead mobility remains low **(**Figures 5 and 7). A possible explanation for the discrepancy is that the fluorescently labeled aptamer has a higher affinity for adenosine than does the unlabeled aptamer, and thus dissociates at lower concentrations. Control measurements performed using 25% labeled aptamer (as opposed to the 1% trace amount used in the experiments above), however, produce effectively identical micron-scale kinetics (Figure S3), ruling out this hypothesis. Other hypotheses we have explored are that the decrease in fluorescence arises due to shear forces (from swelling due to the addition of liquid), or due to photobleaching. The addition of adenosine-free buffer, however, does not substantially alter fluorescence (Figure 2), arguing that these phenomena likewise fail to explain the observed decrease in emission. Given these results, we suspect that the different behavior

observed at high and low effector concentrations arises due to structural rearrangements that occur during slow dissolution. Specifically, studies of organic and biopolymer hydrogels have previously suggested that hydrogel networks can rearrange to distribute their intact crosslinks more evenly, increasing their mechanical strength.[43,44,45] We hypothesize that at sufficiently low effector concentrations the dissociation of the gel is sufficiently slow that similar rearrangements can occur, leading to a network structure that retains relatively high connectivity at lower crosslink densities. More detailed observations and analysis of this discrepancy could form the basis of a further study applying the tools we develop here.

The translation of a molecular-level response to a change in macroscale properties is key to the application of responsive materials in, for example sensors,[9-12] cell entrapment devices,[13] and controlled release systems.[46,47] Given this, the ability to quantitatively probe relationships between molecular- and larger- scale behavior in such materials appears of value. For the entrapment of cells and other particles above the circa hundred-nanometer length scale, for example, our results suggest that responsive hydrogels could show a threshold release type of behavior in which cargo remains entrapped until a given extent of molecular dissolution (due to either sufficient time or target concentration) occurs. Strategies for directly probing molecular- and larger- scale response kinetics may prove still more important for multi-component aptamer-based materials, such as "smart" drug-releasing nanoparticles,[46, 47] and shape-memory hydrogels[8] as the greater complexity of these materials likely renders their properties still less predictable, highlighting the need for their detailed, empirical characterization.

Methods:

Detailed methods and materials are online. Briefly, each Y-DNA monomer three subunit strands that hybridize to form a Y-shaped structure with a double stranded core and pendant single-stranded ends complementary to 7 and 8 bases on the 5' and 3' end of the adenosine-binding aptamer of Huizenga and Szostak.[33] We confirmed the successful synthesis of these monomers *via* an agarose gel (Figure S1). To synthesize the hydrogels we combined 185 μM of each Y-monomer with 485 μM unlabeled aptamer, 4.8 μM Alexa488/Black Hole Quencher-1 labeled aptamer, and 0.002% by volume red Fluoro-Max beads in 60 mM sodium chloride, 20 mM sodium phosphate at pH 7. We imaged the hydrogels in a flow cell consisting of a 1.8 mm diameter, 0.75 mm deep cylindrical well drilled into a glass slide overlain by a polydimethylsiloxane (PDMS) channel consisting of a square hole placed flanked by two 0.8 mm by 20 mm channels (Figure S2). After gel synthesis we covered the well but not the ends of the channel with a PDMS coverslip. After a ~15 minute equilibration period we added 20 μl of adenosine solution to the top of the gel by pipetting it from one side of the channel. For imaging we employed an upright Olympus Fluoroview FV1000 MPE laser scanning confocal microscope with a 25X Olympus X Plan N lens, simultaneously exciting the aptamer fluorophore and fluorescent beads with 473 and 559 nm lasers, respectively, and detecting *via* PMT detectors. Each frame was collected *via* raster scanning with 512 x 512 pixel resolution, and a 1.644 s^{-1} frame rate.

We obtained quantitative aptamer fluorescence decay curves by measuring the average intensity of each frame in the 473 nm channel using ImageJ's batch measure function. We normalized each decay curve to the maximal and baseline fluorescence, which we obtained, respectively, by manually inputting the time of maximal fluorescence (generally at or shortly after the addition of adenosine) and by fitting the last ~50% of the decay curve to a stretched

exponential equation using the Matlab cftool (see SI methods). For plotting we averaged the normalized fluorescence of triplicates. To obtain the time constant of the exponential phase τ we fit the portion of the decay curve after fluorescence had decreased 25% from the maximal value to a simple exponential equation using Graph Pad plotting software. We manually extracted $t_{1/2}$ and t_{lag} for each trace and averaged replicates. We confirmed that labeled and unlabeled aptamer dissociate with similar rates by comparing the micron-scale dissolution rate of gels containing 1% and 25% labeled aptamer **(**Figure S3).

We obtained bead tracks using the particle tracker function on Bitplane Imaris software. We calculated the square change in separation over between two consecutive frames for all pairs of beads present in both frames and separated by a distance less than 10x the bead diameter for the 1.0 and 0.2 μm diameter beads and less than 3x the diameter for the 3 μm beads (see ref[37]), employ this change in separation rather than the position change of individual beads to minimize potential effects from drift (*i.e.*, from microscope or flow channel movement). For plotting and data analysis of bead mobility as a function of time (*i.e.*, as in Figures 4, 5), we binned the squared change in separation for each trial into 50 (14 mM trials) or 100 (all others) chronological bins, then averaged and divided by two to obtain the mean squared displacement (MSD) (see SI derivation 1). For fitting we instead averaged the squared displacements over a single frame and manually extracted $t_{1/2}$ (the time at which the MSD is equal to half that expected in buffer) and t_{lag} (the time at which the MSD is equal to 10% that expected in buffer). We fit the portion of the MSD vs time curves after t_{lag} and fit each to simple time delayed exponential equations in GraphPad to obtain τ. To obtain plots of mean square displacement as a function of fluorescence intensity (*i.e.*, as in Figure 7), we employed the mean square displacements between individual pairs of consecutive frames rather than those binned over

multiple time points, then averaged both mean square displacement and fluorescence intensity at given times for multiple replicates to obtain the curves we plot.

Acknowledgements: We thank M. Raven for training and technical support with imaging, T. Soh for the use of his facilities in the fabrication of the gel holder, and O. Saleh and M. Valentine for helpful discussions. LTWS was supported by the Beckman Scholars program funded by the Arnold and Mabel Beckman Foundation. This work was funded by the Institute for Collaborative Biotechnologies through Grant W911NF-09-0001 from the U.S. Army Research Office. The content of the information does not necessarily reflect the position or the policy of the Government, and no official endorsement should be inferred. We also acknowledge the use of the NRI-MCDB Microscopy Facility and the multiphoton/laser scanning confocal microscopes supported by the NCRR and Office of the Director, National Institutes of Health of the NIH under Award S10RR022585 and S10OD010610 respectively.

Author Information:

Corresponding Author: *Email: kwp@chem.ucsb.edu

Present Address: ‡AJS: Center for Systems and Synthetic Biology, University of Texas at Austin, Austin TX 78705

Supporting Information Available: Supplemental materials, methods, figures, derivation and matlab scripts. This material is available free of charge *via* the Internet at http://pubs.acs.org.

References:

1. Pollard, T. D. The Value of Mechanistic Biophysical Information for Systems-Level Understanding of Complex Biological Processes Such as Cytokinesis. *Biophys J.* **2014**, *107*, 2499-2507.

2. Zlotnick, A.; Mukhopadhyay, S. Virus Assembly, Allostery, and Antivirals. *Trends Microbiol.* **2011**, *19*, 14-23.

3. Jahn, R.; Fasshauer, D. Molecular Machines Governing Exocytosis of Synaptic Vesicles. *Nature* **2012**, *490*, 201-207.

4. Meyers, M. A.; McKittrick, H; Chen, P.-Y. Structural Biological Materials: Critical Mechanics-Materials Connections. *Science*, **2013** *339*, 773-779.

5. Whitesides, G. M.; Grzybowski, B. Self-Assembly at All Scales. *Science* **2002**, *29*, 2418-2421.

6. Um, S. H.; Lee, J. B.; Park, N.; Kwon, S. Y.; Umbach, C. C.; Luo, D. Enzyme-Catalyzed Assembly of DNA Hydrogel. *Nat. Mater.* **2006**, *5*, 797-801.

7. Cheng, E.; Xing, Y.; Chen, P.; Yang, Y.; Sun, Y.; Zhou, D.; Xu, L.; Fan, Q.; Liu, D. A pH-Triggered, Fast-Responding DNA Hydrogel. *Angew. Chem.* **2009**, *121*, 7660-7663.

8. Guo, W.; Lu, C. H.; Orbach, R.; Wang, F.; Qi, X. J.; Cecconello, A.; Seliktar, D.; Willner, I. pH-Stimulated DNA Hydrogels Exhibiting Shape-Memory Properties. *Adv. Mater.* **2015**, *27*, 73-78.

9. Helwa, Y.; Dave, N.; Froidevaux, R.; Samadi, A.; Liu, J. Aptamer-Functionalized Hydrogel Microparticles for Fast Visual Detection of Mercury(II) and Adenosine. *ACS Appl. Mater. Interfaces* **2012**, *4*, 2228-2233.

10. Wei, X.; Tian, T.; Jia, S.; Zhu, Z.; Ma, Y.; Sun, J.; Lin, Z.; Yang C. J. Target-Responsive DNA-Hydrogel Mediated "Stop-Flow" Microfluidic Paper-Based Analytic Device for Rapid, Portable, and Visual Detection of Multiple Targets. *Anal. Chem.* **2015**, *87*, 4275-4282.

11. Zhang, L.; Lei, J.; Liu, L.; Li, C.; Ju, H. Self-Assembled DNA Hydrogel as Switchable Material for Aptamer-Based Fluorescent Detection of Protein. *Anal. Chem.* **2013**, *85*, 11077-11082.

12. Guo, W.; Qi, X.-J.; Orbach, R.; Lu, C.-H.; Freage, L.; Mironi-Harpaz, I.; Seliktar, D.; Yang, H.-H.; Willner, I. Reversible Ag+-Crosslinked DNA Hydrogels. *Chem. Commun.* **2014**, *50*, 4065-4068.

13. Xing, Y.; Chen, E.; Yang, Y.; Chen, P.; Zhang, T.; Sun, Y.; Yang, Z.; Liu, D. Self-Assembled DNA Hydrogels with Designable Thermal and Enzymatic Responsiveness. *Adv. Mater.* **2011**, *23*, 1117-1121.

14. Flory, P. J. Molecular Size Distribution in Three Dimensional Polymers. *J. Am. Chem. Soc.* **1941**, *63*, 3083-3090.

15. Maxwell, J.C. On The Calculation of the Equilibrium and Stiffness of Frames. *Phil. Mag.* **1864**, *27*, 294-299.

16. Stauffer, D.; Coniglio, A.; Adam, M. Gelation and Critical Phenomena. *Adv. Polym. Sci.* **2005**, *44*, 103-158.

17. Broedersz, C.P.; Mao, X.; Lubensky, T.C.; Mackintosh, F.C. Criticality and Isostaticity in Fibre Networks. *Nat. Phys.* **2011**, *7*, 983-989.

18. Mao, X.; Stenull, O.; Lubensky, T.C. Effective-Medium Theory of a Filamentous Triangular Lattice. *Phys. Rev. E* **2013**, 042601.

19. Arbabi S.; Sahimi, M. Elastic Properties of Three-Dimensional Percolation Networks with Stretching and Bond-Bending Forces. *Phys. Rev. B* **1988**, *38*, 7173-7176.

20. Sahimi, M.; Arbabi, S. Mechanics of Disordered Solids. II. Percolation on Elastic Networks with Bond-Bending Forces. *Phys. Rev. B* **1993**, *47*, 703-713.

21. Wyart, M.; Liang, H.; Kabla, A.; Mahedevan, L. Elasticity of Floppy and Stiff Random Networks. *Phys. Rev. Lett.* **2008**, *101*, 215501.

22. Rovigatti, L.; Smallenburg, F.; Romano, F.; Sciortino, F. Gels of DNA Nanostars Never Crystallize. *ACS Nano* **2014**, *8*, 3567-3574.

23. Lin, C.-C.; Metters, A.T. Hydrogels in Controlled Release Formulations: Network Design and Mathematical Modeling. *Adv. Drug Deliv. Rev.* **2006**, *58*, 1370-1408.

24. Narasimhan, B. Mathematical Models Describing Polymer Dissolution: Consequences for Drug Delivery. *Adv. Drug Deliv. Rev.* **2001**, *48*, 195-210.

25. Aufderhorst-Roberts, A.; Frith, W. J.; Donald, A. M. A Microrheological Study of Hydrogel Kinetics and Microheterogeneity. *Eur. Phys. J. E* **2014**, *37*, 44.

26. Larsen, T. L.; Furst, E. M. Microrheology of The Liquid-Solid Transition During Gelation. *Phys. Rev. Lett. E* **2008**, *100*, 146001.

27. Schultz, K. M.; Baldwin, A. D.; Kiick, K. L.; Furst, E.M. Measuring the Modulus and Reverse Percolation Transition of a Degrading Hydrogel. *ACS Macro. Lett.* **2012**, *1*, 706-708.

28. Cingli, H. E.; Rombouts, W. H.; Van Der Gucht, J.; Cohen Stuart, M. A.; Sprakel, J. Equivalent Pathways in Melting and Gelation of Well-Defined Biopolymer Networks. *Biomacromolecules* **2015**, *16*, 304-310.

29. Wehrman, M. D.; Lindberg, S.; Schultz, K. M. Quantifying the Dynamic Transition of Hydrogenated Castor Oil Gels Measured *Via* Multiple Particle Tracking Microrheology. *Soft Matter* **2016**, *12*, 6463-6472.

30. Moschakis, T.; Murray, B. S.; Dickinson, E. On The Kinetics of Acid Sodium Caseinate Gelation Using Particle Tracking to Probe the Microrheology. *J. Colloid Interface Sci.* **2010**, *345*, 278-285.

31. Yu, G.; Yan, X.; Han, C.; Huang, F. Characterization of Supramolecular Gels. *Chem. Soc. Rev.* **2013**, *42*, 6697-6722.

32. Bae, K. H.; Wang, L.-S.; Kurisawa, M. Injectable Biodegradable Hydrogels: Progress and Challenges. *J. Mater. Chem. B* **2013**, *1*, 5371-5388.

33. Huizenga, D. E.; Szostak, J. W. A DNA Aptamer that Binds Adenosine and ATP. *Biochemistry* **1995**, *34*, 656-665.

34. Santalucia, J. R. A Unified View of Polymer, Dumbbell, and Oligonucleotide DNA Nearest-Neighbor Thermodynamics. *Proc. Natl. Acad. Sci. USA* **1998**, *95*, 1460-1465.

35. Zuker, M. Mfold Web Server for Nucleic Acid Folding and Hybridization Prediction. *Nucl. Acids Res.* **2003**, *31*, 3406-3415.

36. Dickerson, R. E. Definitions and Nomenclature of Nucleic Acid Structure Components. *Nucl. Ac. Res.* **1989**, *17*, 1797-1803.

37. Crocker, J. D.; Valentine, M. T.; Weeks, E.R.; Gisler, T.; Kaplan, P.D.; Yodh, A.G.; Weitz, D.A. Two-Point Microrheology of Inhomogenous Soft Materials. *Phys. Rev. Lett.* **2000**, *85*, 888-891.

38. Chan, H. S.; Dill, K. A. Intrachain Loops in Polymers. *J. Chem. Phys.* **1989**, *90*, 492–509.

39. Akcora, P.; Liu, H.; Kumar, S. K.; Moll, J.; Li, Y.; Benicewicz, B. C.; Schadler, L. S.; Acehan, D.; Panagiotopoulos, A. Z.; Pryamitsyn, V.; Ganesan, V.; Ilavsky, J.; Thiyagarajan, P.; Colby, R. H.; Douglas, J. F. Anisotropic Self-Assembly of Spherical Polymer-Grafted Nanoparticles. *Nat. Mater.* **2009**, *8*, 354-359.

40. Mammen M.; Shakhnovich, E. I.; Deutch, J. M.; Whitesides, G. M. Estimating the Entropic Cost of Self-Assembly of Multiparticle Hydrogen-Bonded Aggregates Based on the Cyanuric Acid·Melamine Lattice. *J. Org. Chem.* **1998**, *63*, 3821-3830.

41. Fasting, C. A.; Schalley, M.; Weber, O.; Seitz, O.; Hecht, B.; Koksch, J.; Dernedde, C.; Graf, E.-W.; Haag, R. Multivalency as a Chemical Organization and Action Principle. *Angew. Chemie.* **2012**, *51*, 10472-10498.

42. Ercolani, G. Assessment of Cooperativity in Self-Assembly. *J. Am. Chem. Soc.* **2003**, *125*, 16097-16103.

43. Draper, E. R.; McDonald, T. O.; Adams, D.J. A Low Molecular Weight Hydrogel with Unusual Gel Aging. *Chem. Commun.* **2015**, *51*, 6595-6597.

44. Smith, M. M.; Smith, D. K. Self-Sorting Multi-Gelator Gels – Mixing and Ageing Effects in Thermally Addressable Supramolecular Soft Nanomaterials. *Soft Matter* **2011**, *7*, 4856-4860.

45. Rodríguez-Llansola, F.; Miravet, J. F.; Escuder, B. Supramolecular Gel Formation and Self-Correction Induced by Aggregation-Driven Conformational Changes. *Chem. Commun.* **2009**, *2*, 209-211.

46. Kim, T.; Park, S.; Lee, M.; Baek, S.; Lee, J. B.; Park, N. DNA Hydrogel Microspheres and Their Potential Applications for Protein Delivery and Live Cell Monitoring. *Biomicrofluidics* **2016**, *10*, 034112.

47. Li, J.; Zheng, C.; Cansiz, S.; Wu, C.; Xu, J.; Cui, C.; Liu, Y.; Hou, W.; Wang, Y.; Zhan, L.; *et al*. Self-Assembly of DNA Nanohydrogels with Controllable Size and Stimuli-Responsive Property for Targeted Gene Regulation Therapy. *J. Am. Chem. Soc.* **2015**, *137*, 1412-1415.

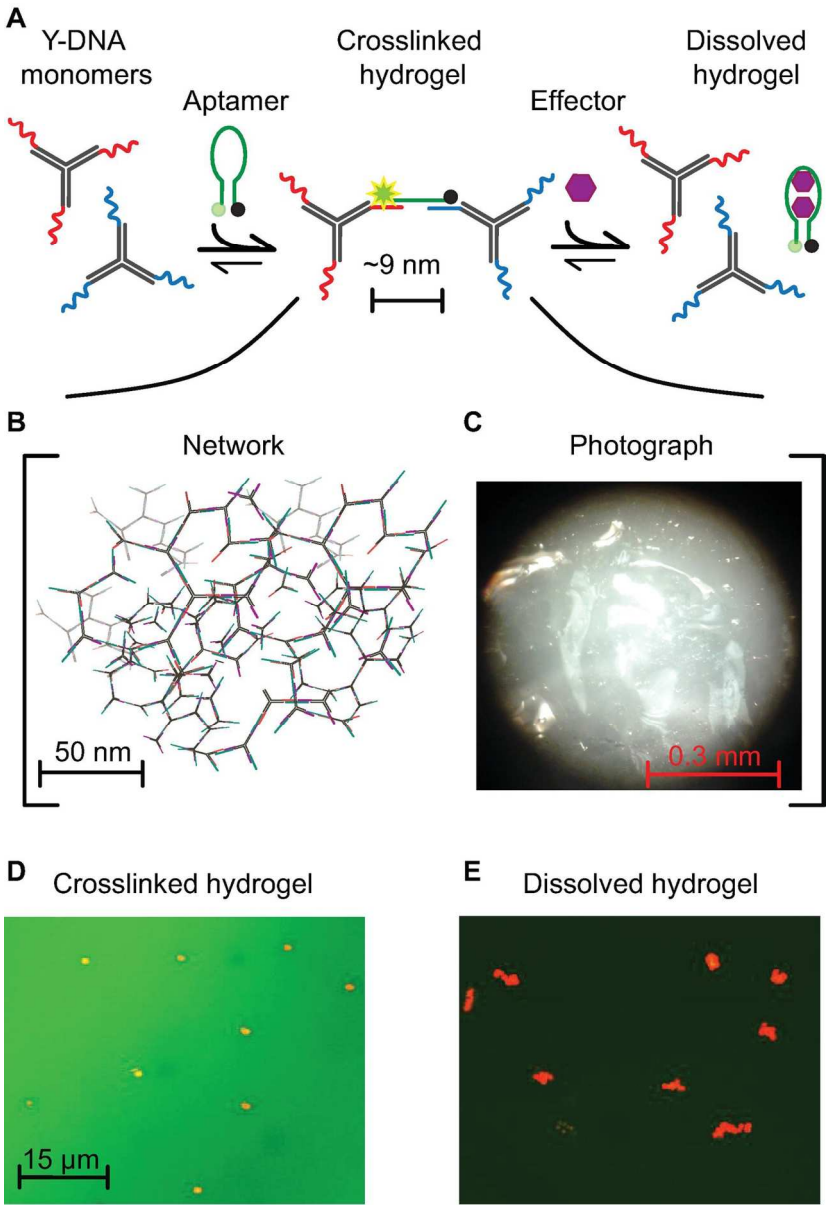

Figure 1. As our model system we employed an adenosine-responsive DNA hydrogel modeled on a Y-DNA hydrogel architecture first described by Cheng *et al.*[7] (A) This consists of Y-shaped "monomers" (each consisting of three annealed strands of DNA) with pendant, single-stranded arms. These arms are partially complementary to a 27-base, adenosine-binding aptamer, which crosslinks the monomers to form a 3-dimensional network (B) that forms a visibly thick gel (C). As each base pair in double stranded DNA contributes ~ 0.3 nm in helical rise, we estimate the length of this aptamer in the extended conformation as approximately 9 nm.36 In response to binding its specific molecular effector, adenosine, the aptamer dissociates and folds, disrupting the hydrogel (D, E). To monitor the dissolution of the hydrogel over molecular and hundred-nanometer length scales we employ a trace of fluorophore/quencher-modified aptamer and embedded, 210 nm to 3.2 μm-diameter fluorescent beads, respectively. This composite image (D) shows the signals arising from the trace of labeled aptamers (green channel) and the beads (red channel) summed over 20 frames (33 s) in the absence of the adenosine effector. Some 25 min after the addition of 14 mM adenosine (E), in contrast, the emission of the fluorophore labeled aptamers is greatly

decreased, and the beads show significant mobility over the 20-frame data collection time.

Figure 1
121x177mm (300 x 300 DPI)

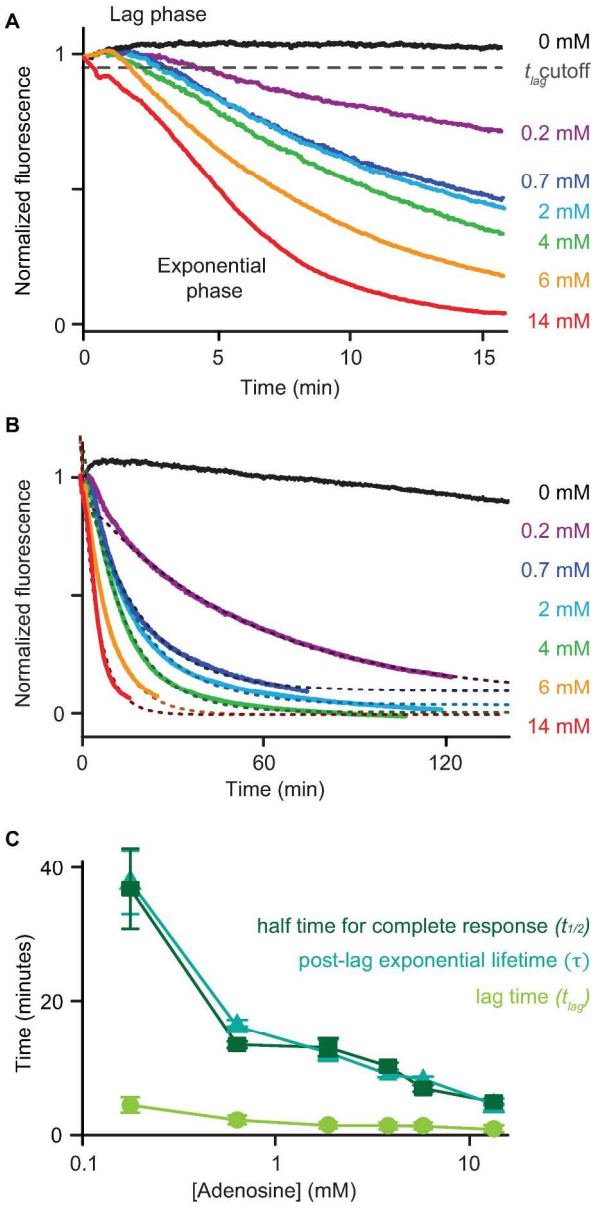

Figure 2. The adenosine-responsive hydrogel exhibits biphasic dissolution kinetics when the dissolution is monitored over molecular length scales. (A) A close-up plot of the first 15 min after the addition of adenosine illustrates the concentration-dependent lag phase in the response of a trace of fluorophore-modified aptamer in the hydrogel. (B) This is followed by a concentration-dependent exponential dissolution phase. Note: we observe near complete dissolution even at the lowest adenosine concentration we have employed. (C) The lag time, t_{lag} (defined here as the time needed to decrease the initial fluorescence by 5%), the lifetime of the exponential phase, τ (determined after the fluorescence has decreased by 25%) and, thus, the half-time of dissolution $t_{1/2}$ all increase monotonically with decreasing adenosine concentration.

Figure 2
162x332mm (300 x 300 DPI)

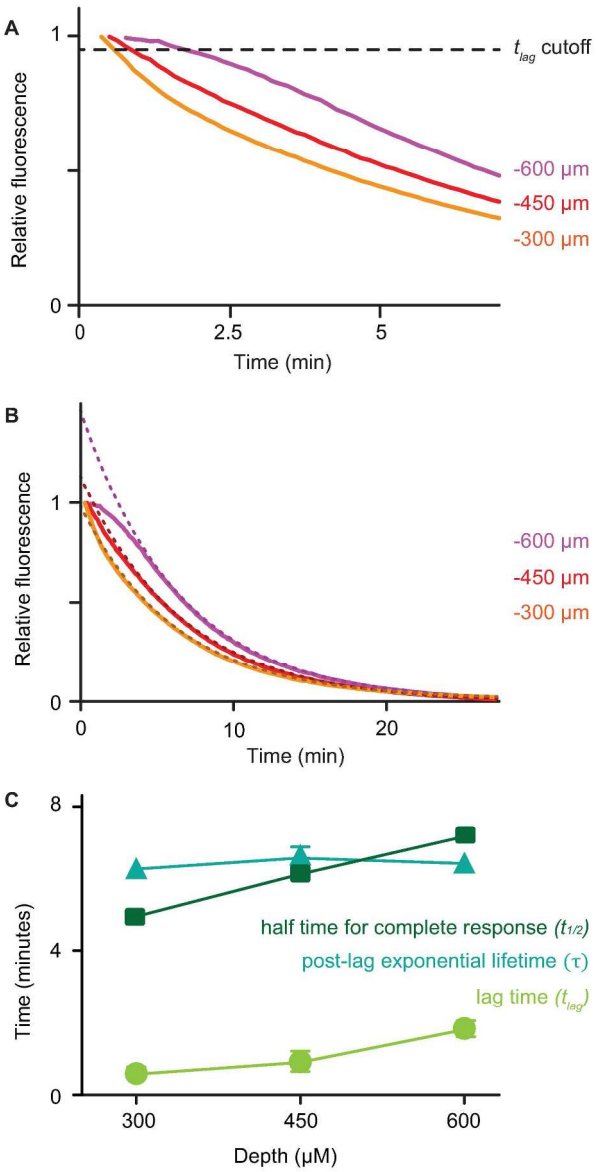

Figure 3. Due to effects on the lag phase, the kinetics of the molecular scale dissolution of DNA hydrogels depends strongly on depth below the surface at which the observations are made. The exponential kinetics observed after the lag phase, in contrast, are effectively independent of depth. (A) The length of the lag phase (defined here somewhat arbitrarily as the length of time before fluorescence decreasing to less than 95% of the starting value, with results and conclusions presented not depending significantly on the choice of this threshold) increases monotonically with increasing depth. (B) After this initial depth-dependent lag phase, the fluorescence decreases with similar kinetics at all depths. (C) The lag time t_{lag} increases from 0.6±0.2 min at 300 µm to 1.8±0.1 min at 600 µm. The lifetime of the exponential phase (fit when fluorescence has decreased by 25%), however, are effectively indistinguishable.

Figure 3
164x318mm (300 x 300 DPI)

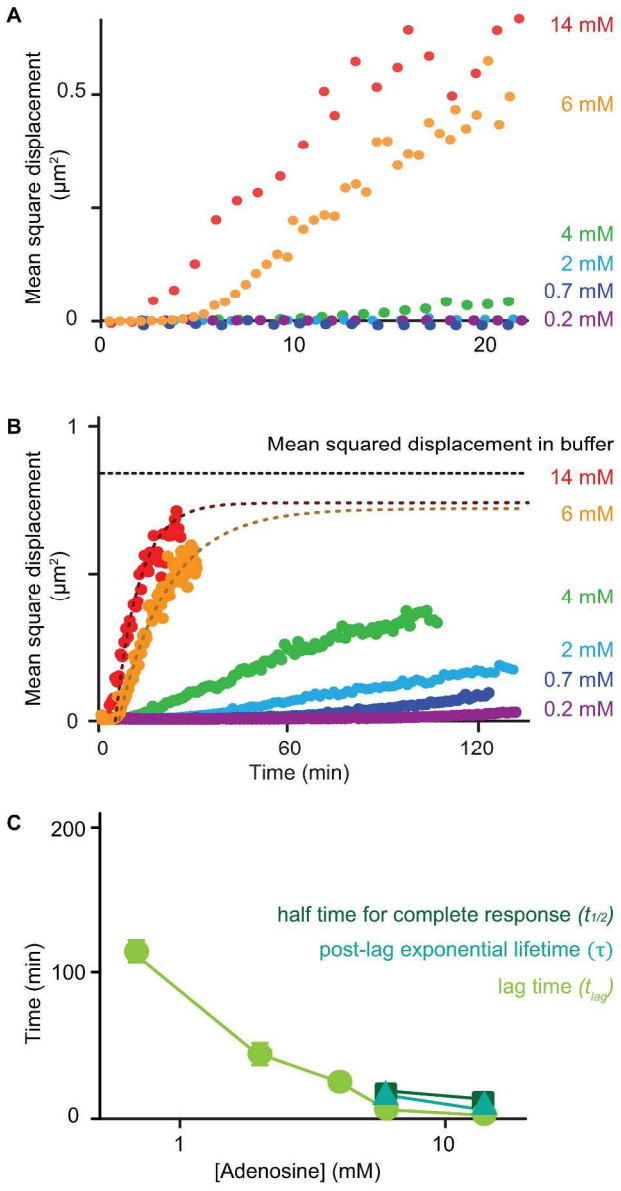

Figure 4. (A) As is true of its molecular scale dissolution, the micron scale dissolution of the hydrogel exhibits biphasic behavior in which an initial lag phase is followed by (B) near-exponential behavior. Notably, very little increase in mobility (here as probed by monitoring the mobility of 1.0 μm-diameter beads) occurs even after 120 min in response to lower than 2 mM adenosine. (C) The lag time increases from t_{lag} = 5.9±0.3 min at 14 mM adenosine to longer than 120 min at 0.2 mM adenosine. The lifetime of the exponential phase ranges from τ = 9.4±1.6 min to τ = 14.0±1.0 min at 14 mM and 6 mM respectively. At concentrations ≤ 4 mM, the bead motion does not reach the plateau value within the experimental time frame, preventing the extraction of characteristic exponential time constants and rendering it difficult to estimate dissolution half-times.

Figure 4
160x300mm (300 x 300 DPI)

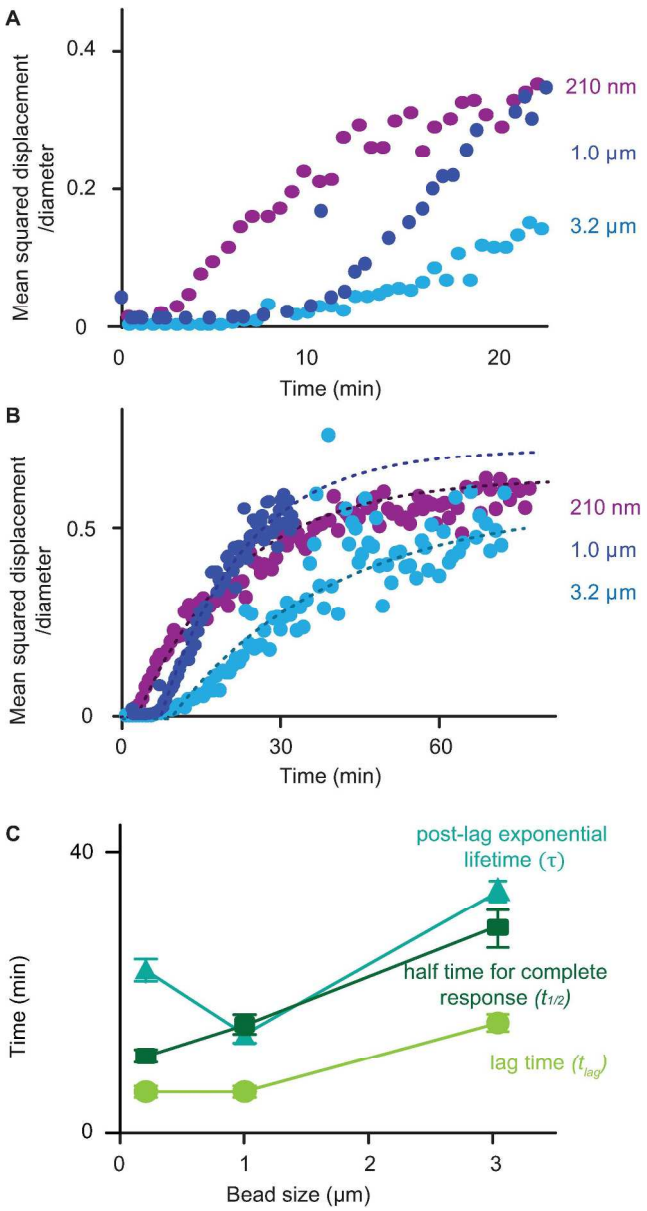

Figure 5. Dissolution measured by 210 nm, 1.0 µm, and 3.2 µm beads, i.e., dissolution measured at these length scales, show a pattern of a lag phase (A) followed by exponential (B) behavior. The curves for smaller beads are shifted to the left, suggesting earlier dissolution at shorter length scales. (C) Quantitatively, the lag time increases about twofold from t_{lag} = 5.5±0.8 min for 210 nm beads to t_{lag} = 15.8±1.4 min for 3.2 µm beads. Likewise, the lifetime of the exponential phase increases with increasing bead size, from τ= 23.0±1.5 min for 210 nm beads to τ= 34.8±2.9 min for 3.2 µm beads.

Figure 5
159x300mm (300 x 300 DPI)

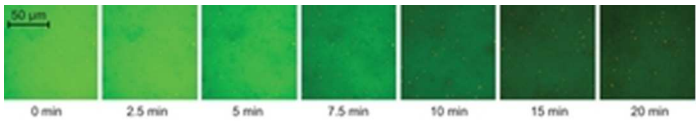

Figure 6. Sequential images of a single region of a dissolving hydrogel show a homogeneous decrease in aptamer fluorescence over time (green), indicating that dissolution is spatially uniform in the x-y plane over micrometer dimensions. This stands in contrast to patchier, nucleation-like dissolution (in which small initial areas of dissolution form and expand) or wave front dissolution (in which dissolution occurs as a front advancing from one side). The latter observations might be expected were the dissolution process to be cooperative.

Figure 6
29x4mm (300 x 300 DPI)

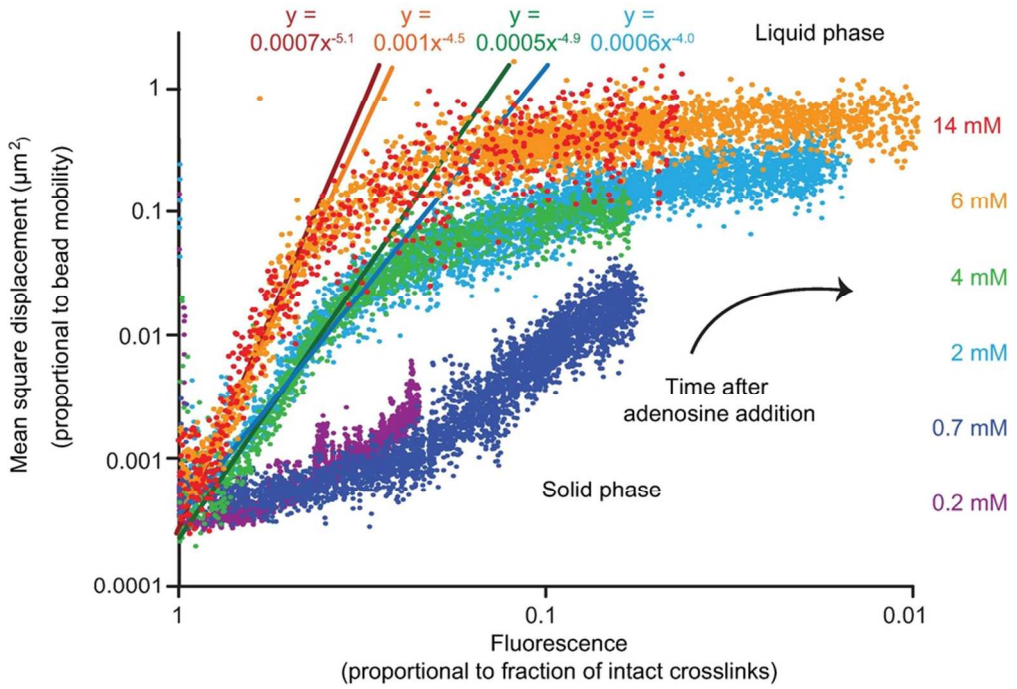

Figure 7. At adenosine concentrations above 2 mM plots of the fluorescence of the labeled aptamer (a proxy for the fraction of intact crosslinks remaining) versus the mean squared displacement of the beads during dissolution reveals a biphasic transition from solid-like to liquid-like behavior. The mean square displacement (measuring micron-scale dissolution) versus fluorescence (molecular-scale dissolution) at 2, 4, 6, and 14 mM adenosine exhibit an initial power law phase with fit characteristic exponents near the predicted[19, 20] value of ~3.8. Also as predicted by theory, the solid-to-liquid transition occurs when approximately 50% of the molecular bonds are broken.[14] At lower adenosine concentrations, in contrast, the micron-scale dissolution versus molecular-scale dissolution relationship is shallower and does not show this clear transition. This suggests that, under these conditions, dissolution may occur through a different mechanism.

Figure 7
84x57mm (300 x 300 DPI)

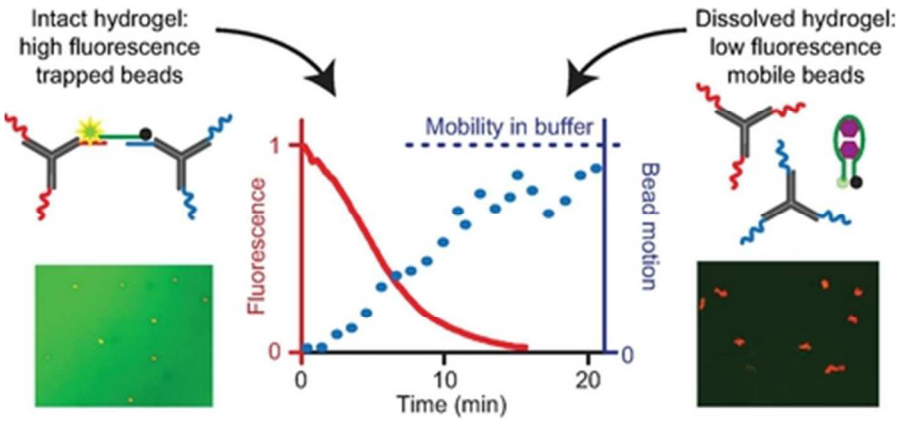

DNA's base-pairing rules support the construction of stimulus-responsive materials with controllable thermodynamics and kinetics, but our ability to control such properties is limited by a lack of simple tools for their measurement. We demonstrate a straightforward, time-resolved, and multi-scale technique for measuring DNA hydrogel dissolution and apply it to determine the concentration-, position-, and length-scale dependence of the response of a model hydrogel, finding behaviors consistent with theoretical predictions.

Table of contents graphic
37x17mm (300 x 300 DPI)